

**Search for Neutrino Oscillations at the AGS
with the Narrow Band Beam⁺**

C. Chi, N. Kondakis, W. Lee, B. Rubin, R. Seto,
C. Stoughton, G. Tzanakos
Physics Department, Columbia University

E. O'Brien, T. O'Halloran, K. Reardon, S. Salman
Department of Physics, University of Illinois
1110 West Green St., Urbana, Illinois 61801

B. Blumenfeld, L. Chichura, C. Y. Chien, J. Krizmanic,
E. Lincke, W. Lyle, L. Lueking, L. Madansky, A. Pevsner
Department of Physics and Astronomy,
The Johns Hopkins University

(Presented by G. Tzanakos)

Abstract

We have taken neutrino data with the NBB at BNL, in the summer and fall of 1985, and with the WBB in the spring of 1986. We are in the process of completing the analysis of the NBB data. In this paper we present preliminary results of this analysis. We observe an anomalous appearance of electron neutrinos above the expected background.

(⁺) This paper is based on additional analysis done since the workshop.

Presented at the BNL Neutrino Workshop,
February 1987.

MASTER

1. Introduction

If neutrinos have a non-zero mass and if the flavor lepton numbers are not independently conserved, then neutrinos can oscillate from one flavor to another, provided that at least two of the masses are different. Assume, for simplicity, two neutrino flavors, ν_μ and ν_e . The probability for the transition $\nu_\mu \rightarrow \nu_e$ is:

$$P = \sin^2 2\alpha \cdot \sin^2 \left(1.27 \frac{\Delta m^2 \cdot L}{E_\nu} \right), \quad (1)$$

where

α = the flavor mixing angle;

L = distance from the neutrino source in km;

E_ν = neutrino energy in GeV;

$\Delta m^2 = |m_1^2 - m_2^2|$ in eV^2 ;

m_1, m_2 = the masses of the mass eigenstates.

We built a neutrino experiment at $L = 1$ km from the neutrino source of a narrow band beam of mean energy $E_\nu = 1.27$ GeV and spread $\sigma_E/E = 15\%$, to search for the $\nu_\mu \rightarrow \nu_e$ oscillation.

Our experiment (E776) ran during the past two years, collecting the following data:

NBB run	3×10^{19} POT	Summer, Fall 1985
WBB run	3×10^{19} POT	Spring 1986
TEST (Calibration)		Summer 1986

A brief description of the detector and the narrow band beam follows. We will also describe the data taking, data reduction, and analysis of ν_μ and ν_e events, including a discussion of the backgrounds. Finally, very preliminary results from this analysis will be presented.

2. The Detector

The detector¹ is located at 1 Km from the target along the neutrino line as shown in Fig. 1. It is composed of two sections, the front 'electron detector', which is a finely segmented EM calorimeter, followed by a toroidal magnetic muon spectrometer. A schematic of the detector along with some details is shown in Fig. 2.

The Electron detector is made up of nine sections. Each section is made of 10 planes of proportional drift tubes (PDT), interleaved with absorber planes made of 1" concrete. The last concrete plane in every section is replaced by a scintillator plane, used for timing and cosmic ray triggering. Sequential PDT

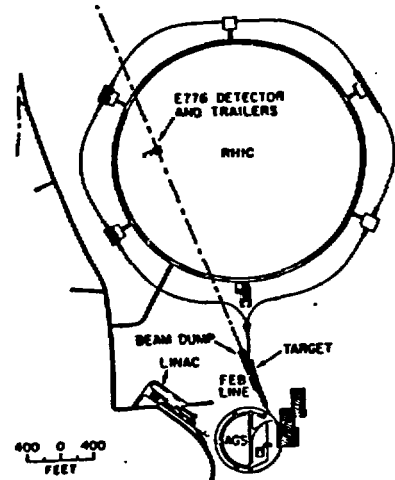


Fig. 1. Location of the E776 detector in the AGS neutrino line.

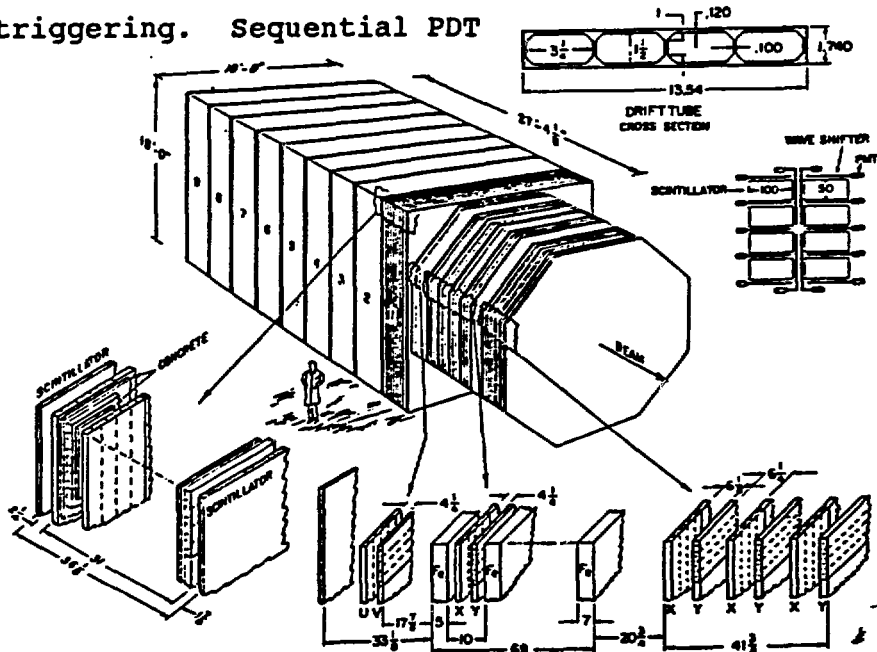


Fig. 2. E776 detector schematic.

planes are at 90 degrees with respect to each other. Each PDT plane contains sixty-four $18 \times 3 \frac{1}{4} \times 1 \frac{1}{2}$ " drift tubes, made of extruded aluminum, with four PDTs per extrusion. The maximum drift distance is 4.1 cm. The sampling interval is $\frac{1}{3} X_0$, and the weight is 240 metric tons (120 tons fiducial). Each PDT signal is amplified and carried to the input of a 6-bit 22.4 ns flash ADC, connected to a 6x256 bit memory, which allows the $5.7 \mu\text{s}$ latest history of the wire pulse to be recorded.

The muon spectrometer is composed of five iron toroids: there are two planes of PDT's (1X,1Y) between sequential toroids, and six (3X,3Y) PDT planes after the last toroid. The total thickness of the iron is 29" and the magnetic field is about 18 kG, resulting in a P_T kick of 400 MeV/c.

A typical muon neutrino event is shown in Fig. 3a with the muon track exiting through the toroid system. The reconstructed muon trajectory is shown in Fig. 3b. The spatial resolution of the detector is $\sigma_x = 2 \text{ mm}$, and the angular resolution of the muon tracks at the vertex is approximately 25 mrad. The momentum resolution, σ_p/p ,

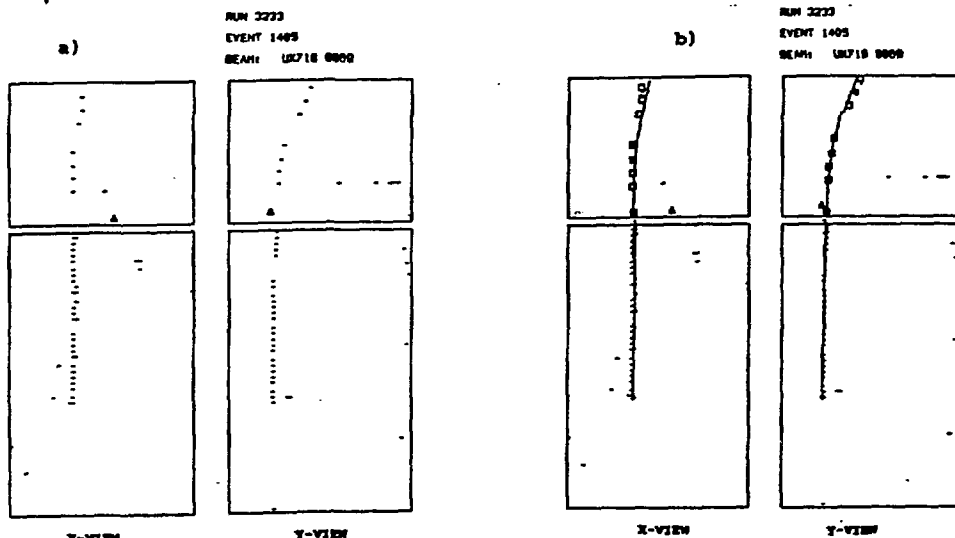


Fig. 3. Typical candidate for quasielastic ν_μ interaction, with muon penetrating the toroid. a) Raw data. b) Reconstructed muon track; $p_\mu = 2.5 \text{ GeV/c}$.

for muon tracks is on the order of 5% for muons stopping in the electron detector, 10% for muons stopping in the toroids, and 25% for tracks exiting the toroids. The detail of the wire pulses, as digitized by the flash ADC's, is shown in Fig. 5b, for ten sequential planes of x-wires.

Fig. 4 shows an electron neutrino quasielastic candidate. Our criteria for electromagnetic shower development include multiple hits per plane, and missing hits in several planes. The most striking feature is the structure and size of the digitized wire pulses. Fig. 5a shows the wire pulses for ten sequential x-planes. The multiple peaks in the pulses and the dramatically increased pulse areas reflect the fact that several shower particles cross each drift tube. A comparison between Figs. 5a and 5b shows a pronounced difference between electrons and muons as seen by the detector.

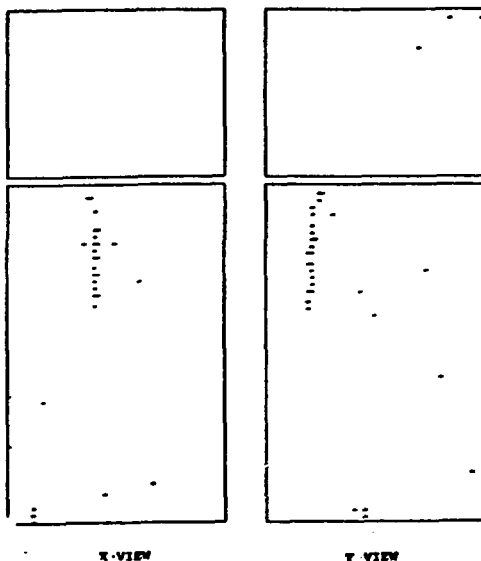


Fig. 4. Typical candidate for quasielastic ν_e interaction.

We constructed a small (8 ton) detector and took calibration data in the A2 test beam at the AGS. We exposed this test detector to electrons, stopping muons, stopping pions, and stopping protons of various energies. We measured the e/μ , e/π^\pm , and e/p separation in the detector. The electron identification exploits the longitudinal and lateral development characteristics of the shower.

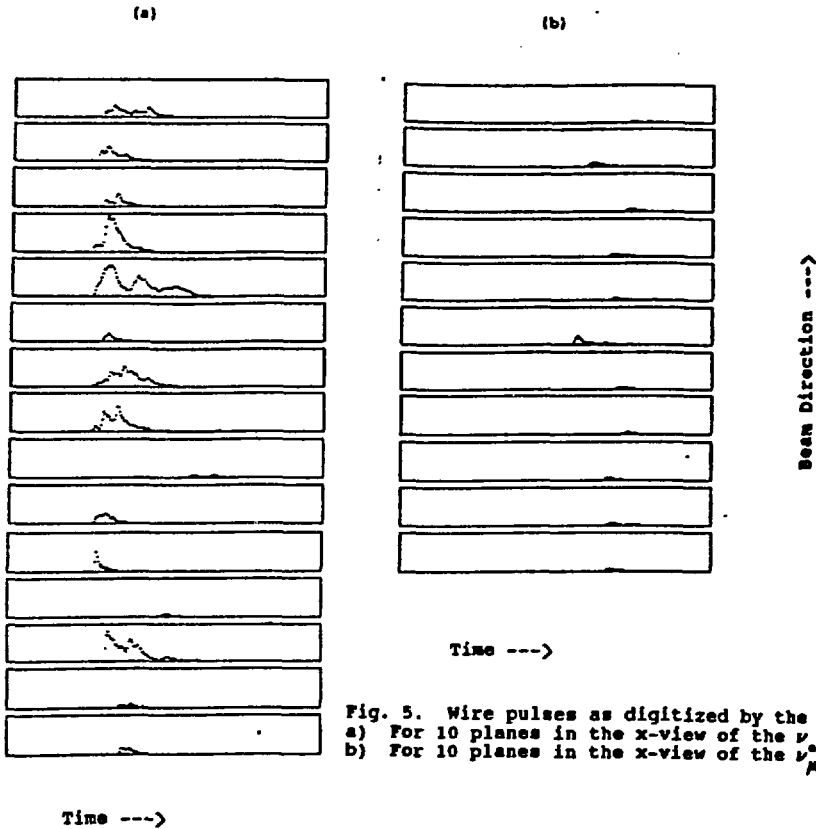


Fig. 5. Wire pulses as digitized by the flash ADCs.
 a) For 10 planes in the x-view of the ν candidate (Fig. 4).
 b) For 10 planes in the x-view of the ν_μ candidate (Fig. 3).

The average longitudinal shower behavior can be described by the equation:

$$N(E) = N_0(E) t^a e^{-bt}, \quad (2)$$

where t is the shower depth in radiation lengths, and

$$\begin{aligned} N_0(E) &= 5.51 E \sqrt{Z} b^{a+1} / \Gamma(a+1); \\ a &= 1.77 + 0.52 \ln E; \\ b &= 0.634 - 0.0021 Z. \end{aligned} \quad (3)$$

The shower maximum occurs at depth $t = a/b$. Fig. 6 shows the longitudinal energy deposition profile for the test detector along with the curve given by Eq. (2). The agreement demonstrates clearly that the shower development in our detector is what we expect.

The shower development, however, fluctuates from this average behavior on an event by event basis. We exploit these fluctuations in order to separate electrons from other particles.

We also calculated the energy calibration constant for electron showers in the neutrino detector with the data from the test detector. The measured pulse areas were

corrected for gain variations due to changes in temperature, pressure, and gas composition, which were monitored by studying cosmic ray tracks taken between AGS spills. Fig. 7 shows a plot of the electron energy as measured by the detector versus the energy of the beam, for electrons entering the detector at $\theta = 0^\circ$, and $\theta = 30^\circ$. It is clear that the response of the calorimeter is linear with energy and independent of the direction of the shower. The same

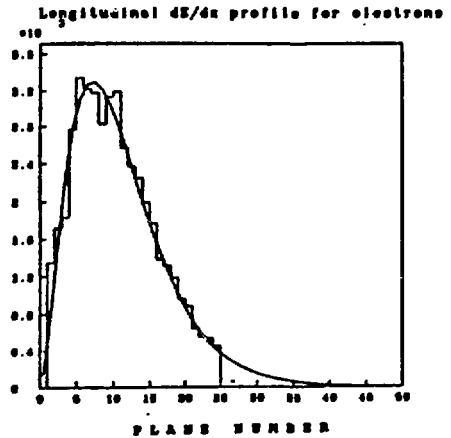


Fig. 6. Longitudinal shower energy profile for 1 GeV electrons. The curve is given by Eq. 2 in the text.

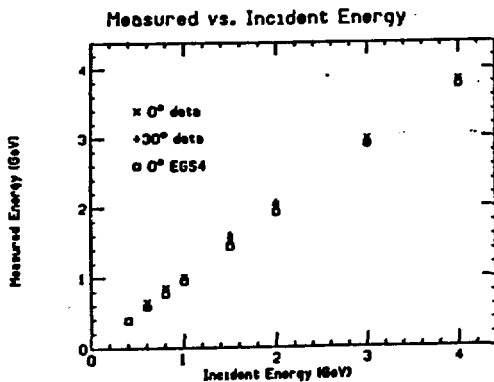


Fig. 7. EM calorimeter (test detector) response vs. true electron energy.

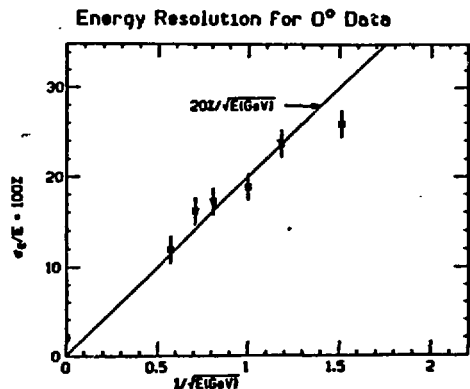


Fig. 8. EM calorimeter energy resolution vs. $1/\sqrt{E}$.

figure also shows the simulated response of the calorimeter to electrons generated with the EGS4² electron shower generator program. We measured the energy resolution σ_E/E using the A2 test beam data, which is plotted against $1/\sqrt{E}$ in Fig. 8. The energy resolution is consistent with $20\%/\sqrt{E}$. In conclusion, the results obtained from this test data demonstrate that we understand the behavior of the detector.

3. The Narrow Band Neutrino Beam

We use a narrow band beam in this experiment for the following reasons:

(i) The energy spectrum of the ν_μ 's from oscillation is given by the narrow band spectrum of the parent ν_μ 's, modified by Eq. (1). In contrast, the ν_μ component of the beam has a wide band energy spectrum.

(ii) The high energy part of the spectrum, which gives rise to high topology deep inelastic scattering events, is reduced in the narrow band beam.

The AGS neutrino beamline consists of the proton beam transport, the target, and the magnetic focusing horns, followed by 80 meters of decay space in the beam tunnel, and the muon shield (30 m of iron). The focused beam intensity profile is measured by two sets of planar segmented ionization chambers (pion monitors) at 40 m and 60 m from the second horn.

The details of the magnetic horn calculations, as well as the corresponding beam measurements, are presented in another paper³ given in this workshop. Here we summarize these results. Fig. 9 shows the calculated ν_μ energy

spectrum. The narrow band pion and kaon decay contributions are shown sitting on a falling wideband background due to decays of the non-focused part of the beam. On the same figure the ν_μ beam background is also plotted versus neutrino energy.

This background is mainly due to K_{e3} decays, muon decays, K^0 decays, and π_{e2} decays, which are shown in Fig. 10. The total ν_μ/ν_μ ratio of the beam was calculated to be at the 8×10^{-3} level with an estimated error of 30%.

The energy spread of the narrow band beam is $\sigma_E/E = 15\%$, and the angular spread of the charged beam is 4 mrad.

In order to verify the beam calculation, we compared its predictions with the measurements of (i) the total charged particle flux and beam profile in the decay tunnel (measured with the pion monitors) and (ii) the ν_μ energy spectrum and rates in the detector. We used the ν_μ flux given by the beam calculation and known cross sections to generate Monte Carlo ν_μ events. With the muon neutrino analysis discussed below, in section 5.1, we generated the Monte Carlo spectrum shown in Fig. 12, which we compare to the observed ν_μ

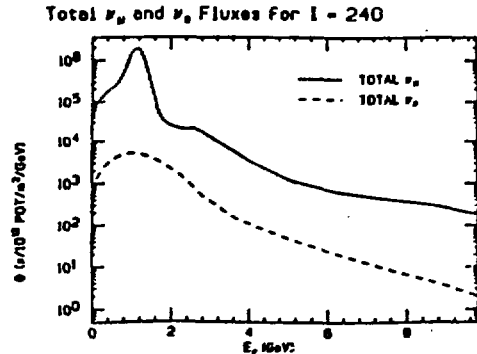


Fig. 9. NBB ν_μ energy spectrum from π^+ and K^+ decays. The WBB background contribution is included. The total ν_μ background in the beam is shown also for comparison.

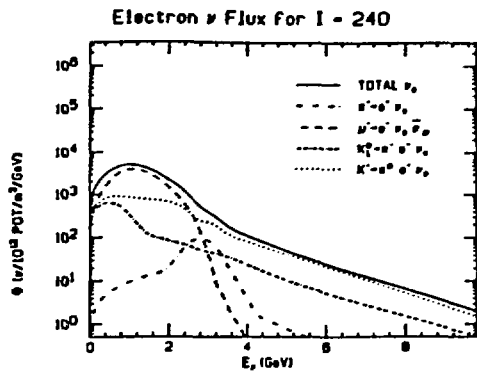


Fig. 10. Energy spectra of the most dominant contributions to the ν_μ background in the beam.

spectrum. From these comparisons, we conclude:

i) The measured flux of charged particles in the beam tunnel and the measured neutrino rates at the detector are both 30% higher than the prediction from the beam calculation. This prediction is based on the model of Sanford and Wang, as discussed in the paper on the neutrino flux calculation.

ii) The measured beam profiles, shown in Fig. 11, agree with the calculated beam shape, once the absolute beam flux normalization is taken into account.

iii) The measured ν_μ spectrum, shown in Fig. 12, agrees with the spectrum of Monte Carlo generated ν_μ events. In this figure, the number of events in the Monte Carlo is normalized to the number of events in the data below 2 GeV. The spectra peak at 1.3 GeV, as expected for $I_{\text{HORN}} = 240$ kA, and the widths are both $\sim 23\%$.

iv) The measured spectrum has \sim two times as many events above 2 GeV as the Monte Carlo spectrum. We are currently investigating sources of this excess.

a) Additional channels in the event generation, such as multi-pion production or deep inelastic scattering, contribute additional events in the high energy tail of the Monte Carlo spectrum. Although we attempt to select quasielastic interactions, these additional channels contribute to the observed spectrum.

b) The reconstruction of high energy muon tracks, which exit the toroid system, has non-gaussian errors. This contributes to the observed number of events in the high energy tail.

This excess appears to be within the limits of the beam calculation and event reconstruction uncertainties. However, we are also investigating additional contributions to the WBB background, through the development of a more sophisticated beam flux calculation. We do not expect the ν_e/ν_μ ratio to change appreciably.

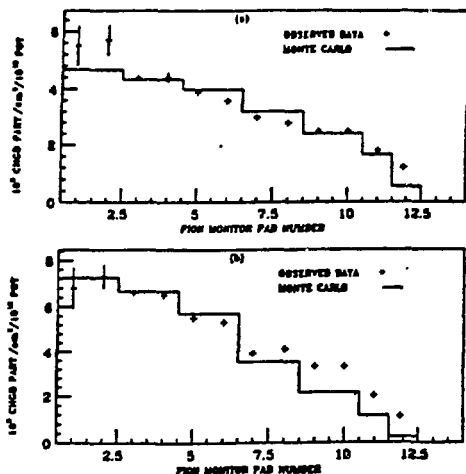


Fig. 11. Charged beam profile, as measured with the pion monitors in the decay tunnel. The calculated beam profile is shown for comparison. a) Downstream monitor. b) Upstream monitor

ν_μ Data and MC Spectra for I = 240

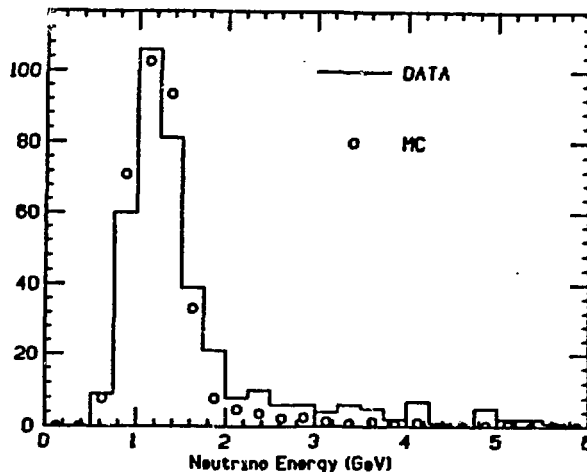


Fig. 12. The measured ν_μ energy spectrum from quasielastic neutrino events compared with the energy spectrum from Monte Carlo generated events.

4. The NBB Run

We collected data during the Summer and Fall of 1985 at two neutrino energies: 1.3 GeV ($I_{\text{horn}} = 240 \text{ KA}$) and 1.5 GeV ($I_{\text{horn}} = 280 \text{ KA}$), accumulating 3×10^{19} POT (protons on target). Three different types of records were written on tape: "beam", "free", and "cosmic" triggers. The beam trigger covered the 2.4 μsec beam spill; this trigger contains the neutrino induced events. The maximum drift time in the PDT's is about 2 μs . Thus, the flash ADC time range of 5.7 μs covered the beam spill very conveniently. The "free" trigger read out the detector between spills for a time interval equal to the beam trigger, to monitor the accidental background from cosmic rays. The "cosmic" trigger, generated by a programmable processor using the scintillation detectors, was used to monitor and calibrate the detector.

4.1 Data Reduction

We collected 2.6×10^6 beam triggers, 2.6×10^6 free triggers, and 1.5×10^6 cosmic triggers during the NBB run. The data tapes were reduced by a series of software filters designed to progressively select the neutrino candidates. Filter 1 separated the cosmic triggers to a separate tape and reduced the beam and free triggers by keeping events with clusters of three or more hits. Filter 2 selected only the neutrino-like events, namely, events with a vertex in the detector. Filter 3 selected those events with at least one contained track and, in the case of showers, a minimum shower energy of 300 MeV. Filter 4 essentially made fiducial and minimum energy cuts and selected fully contained events, for which one can, in principle, calculate the neutrino energy. This filter accepted an event as either an electron candidate (Filter $4e$) or as a muon candidate (Filter 4μ). Table I shows the event reduction through these filters.

Table I

Raw events	2.6 M	Beam triggers
	2.6 M	Free triggers
Filter 1	454	K
Filter 2	38.3	K
Filter 3	12.8	K
Filter 4μ	2388	ν_μ candidates
Filter $4e$	1653	ν_e candidates

5. Analysis

After the filtering process we were left with 2388 ν_μ candidates and 1653 ν_e candidates. The analysis started

with this event sample. Each neutrino candidate was scanned and in each event we assigned hits to 'tracks' with the help of an interactive computer program. Complex events were not used in this analysis.

Each track was identified as e , γ , μ , hadron, or "unknown". These tracks were matched in both views. The next step in the analysis was to calculate the kinematical variables for each track, as discussed below. Once the lepton energy and direction were known the neutrino energy was calculated, under the assumption that the interaction was quasielastic, on a stationary neutron.

The event time, as measured by the scintillation counters and the beam Cerenkov counters, was used to separate the neutrino events from out-of-time background. Fig. 13 shows the time structure of raw neutrino events. The twelve buckets, 224 ns apart, reflect the rf structure of the beam.

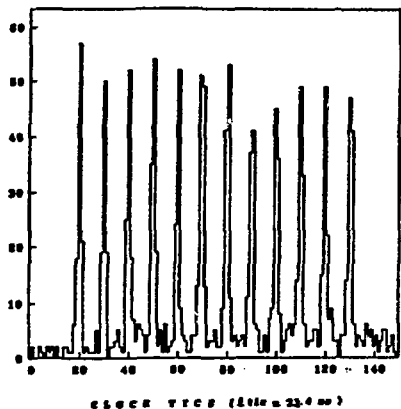


Fig. 13. Raw neutrino event time as measured with the scintillator. The twelve-bucket structure reflects the RF structure of the proton beam.

5.1 Muon Neutrino Analysis

The muon energy measurement was possible if the track stopped in either the electron detector or the toroids, or if it exited the toroids. For a stopping track, the energy was calculated from its range, whereas for exiting tracks

we fit the track through the toroid magnetic field and calculated its momentum. In both cases we developed an algorithm that resolved L-R ambiguities and reconstructed the track by χ^2 techniques, taking into account measurement errors and multiple Coulomb scattering. To determine the muon angle, we used approximately the first one-third of the hits in order to optimize the angular resolution.

In order to obtain the final ν_μ energy spectrum we applied several cuts: beam quality, beam time, event containment, vertex fiducial containment, muon angle, and event multiplicity. After these cuts we were left with 682 ν_μ events. The ν_μ energy distribution is shown in Fig. 14. The cosmic ray background contamination of this sample was calculated by using the free triggers and found to be 8 events. Thus, we are left with a final sample of 674 ν_μ events. Of 10,000 Monte Carlo generated ν_μ interactions, 1207 were accepted through this analysis, giving the ν_μ acceptance of 12%.

Observed ν_μ Spectrum for I = 240, 280

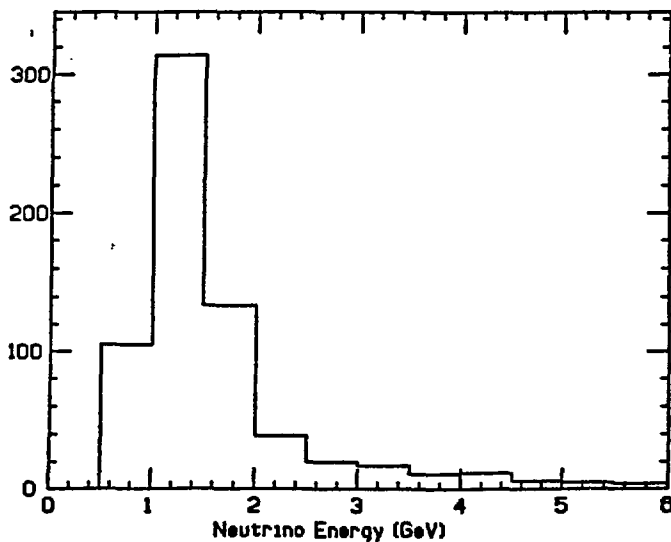


Fig. 14. Measured ν_μ energy spectrum from quasielastic neutrino events, for data taken with $I_{\text{HORN}} = 240$ and 280.

5.2 Electron Neutrino Analysis (present status)

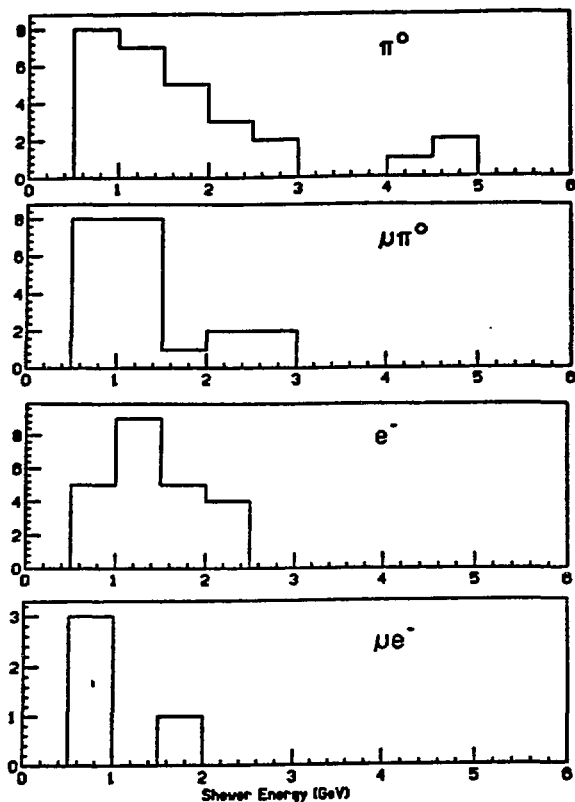
The electron neutrino analysis involves the following steps: i) electron pattern recognition, ii) separation of electrons from π^0 's, iii) estimation of the π^0 background in the electron sample, and iv) estimation of the beam electron neutrino background in the final neutrino sample. The sample of 1653 ν_e candidates from the data reduction (filter 4e) was further reduced by a series of scans performed by physicists. The first of these scans simply selected events with any shower activity in either view, based on a set of selection rules that were tested with Monte Carlo generated events. If either of the two scanners accepted an event, it was retained. In all of the events, hits were assigned to tracks in the way discussed previously. Non-measurable events were not analyzed. A final scan was performed in order to classify the showers into the following types: "no shower", "electron"-, and " π^0 "-like showers. Thus, in the final analysis each event was assigned to one of the following categories:

- i) " π^0 ", a π^0 -like shower and no muon track;
- ii) " $\mu\pi^0$ ", a π^0 -like shower and a muon track;
- iii) "e", an electron-like shower and no muon track;
- iv) " μe ", an electron-like shower and a muon track.

The number of events in each of these categories is given in Table II. This table summarizes the results of the final scan of the data sample. The energy distribution of the showers are shown in Fig. 15 for each of the four classes of events.

Table II

	π^0	$\mu\pi^0$	e	μe
Data	28	21	23	4

Fig. 15. Shower energy distribution for ' π^0 ', ' $\mu\pi^0$ ', 'e', and ' μe ' events.

To understand the significance of the number of ν_μ candidates we observe, two backgrounds must be considered: background from ν_μ induced events, which is dominated by π^0 production, and the ν_μ component of the beam.

a. π^0 Background. The π^0 background arises from muon neutrino induced interactions

$$\nu_{\mu} + N \rightarrow \mu^{-} + \pi^0 \quad (+ X) \quad (4)$$

$$\text{and} \quad \nu_{\mu} \rightarrow \nu_{\mu} + \pi^0 \quad (+ X) \quad (5)$$

These can appear as

$$\nu_{\mu} + N \rightarrow \mu^{-} + e \quad (+ X) \quad (6)$$

$$\nu_{\mu} \rightarrow \nu_{\mu} + e \quad (+ X) \quad (7)$$

whenever one of the gammas is not seen, due to very low energy, or when the two gammas are on top of each other, making the π^0 appear as an electron in the detector. It should be noted that the reactions (5) and (7) include CC events in which the muon is not seen, in addition to the NC events.

The π^0 background is calculated from the number of CC events in the data where a π^0 was identified as an electron. The channel " μe " contains events where a muon was clearly identified, and the shower from a π^0 produced in the interaction was identified as an electron. The ratio, then, of the number of " μe " events to the number of " $\mu\pi^0$ " events is a measure of the probability that a π^0 shower is misidentified as an electron shower. From the neutrino data, this ratio is 4/21. The ratio of the number of " $\mu\pi^0$ " events to the number of " π^0 " events is 21/28, which is consistent with the Monte Carlo prediction. From Table II, the number of background π^0 's in the sample of 23 electron events is:

$$(4/21) \times 28 = 5.3 \pm 3.8 \text{ events.}$$

b. Beam Background. To calculate the background due to the ν_e contamination in the beam, we use the observed number of ν_μ interactions, the calculated ν_e/ν_μ ratio $f_B = 8 \times 10^{-3}$ from the beam calculation, and the relative acceptance of ν_μ and ν_e events. The number of ν_e from the beam is

$$N_e = N_\mu \times f_B \times (A_e/A_\mu). \quad (9)$$

The error in the ratio f_B is estimated to be 30%. From the ν_μ analysis, we saw that 674 events were observed, with an acceptance of 12%. Of 500 Monte Carlo generated ν_e interactions, 76 were accepted, giving an acceptance for ν_e of 15%. Thus, the acceptance ratio $A_e/A_\mu = 1.3$, with an error of 10%. For 674 ν_μ events we can calculate the beam ν_e background in the sample of 23 events to be 7.8 ± 3.8 events.

6. Preliminary Results

The calculated neutrino energy distribution of the electron candidates is shown in Fig. 16, along with the spectra for ν_μ induced π^0 events measured in the data, and the beam ν_e energy spectra. These background spectra have been normalized, for $E_\nu > 0.5$ GeV, to the calculated number of background events in each channel. The energy of the neutrino for the π^0 events was calculated assuming a π^0 to be an electron. It is clearly shown that the observed ν_e spectrum and the background spectra are quite different. In addition, a linear combination of the two background sources gives a spectrum which is different from the ν_e spectrum.

The total number of electron candidates is 23. The number of ν_μ interactions faking ν_e interactions, due to π^0 production, is 5.3 ± 3.8 . The number of ν_e interactions due to the ν_e contamination in the beam is 7.8 ± 3.8 . So we expect to observe 13.1 ± 5.4 events due to the beam and π^0 backgrounds.

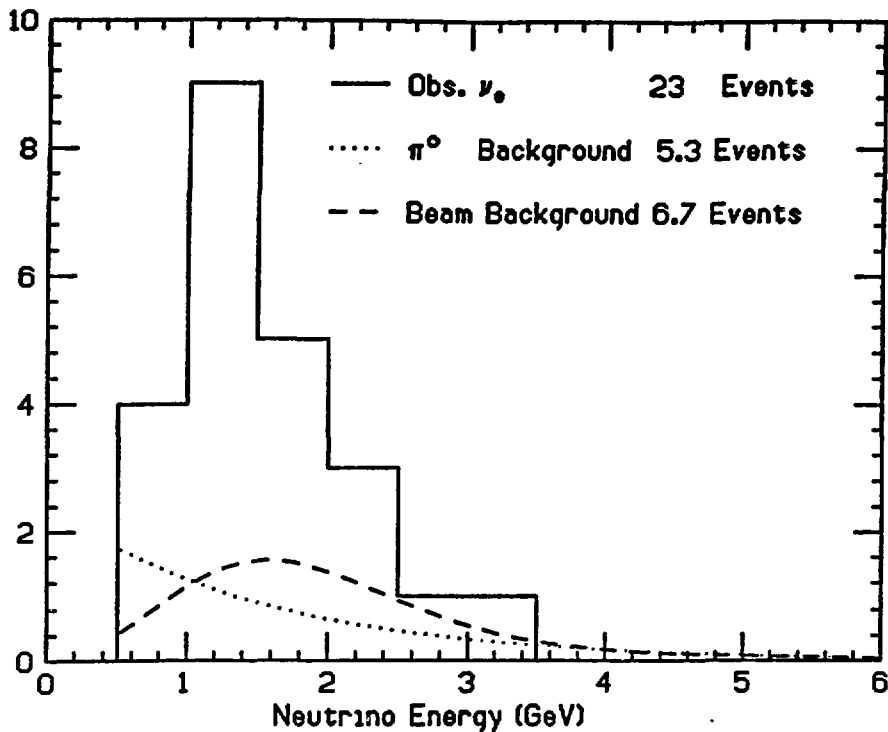
Observed ν_e and Background Spectra

Fig. 16. Measured ν_e energy spectrum for quasielastic events. The background spectra are normalized to contain the expected number of events above 0.5 GeV.

If we limit our analysis to those events between the neutrino energy of 0.6 and 2.3 GeV, the results have more significance. The number of background and observed events in the entire spectrum, and in the peak of the beam spectrum, are summarized in Table III.

Table III

Low Energy Cut	0.5 GeV	0.6 GeV
High Energy Cut	10.0 GeV	2.3 GeV
Observed ν_e	23	20
π^0 Background	5.3 ± 3.8	3.4 ± 2.7
Beam ν_e/ν_μ	$9.3 \times 10^{-3} \pm 30\%$	$6.6 \times 10^{-3} \pm 30\%$
Observed ν_μ	674	579
Beam Background	7.8 ± 3.8	4.5 ± 2.6
Total Background	13.1 ± 5.4	7.9 ± 3.7
Excess ν_e Events	9.9	12.1

The beam ν_e/ν_μ ratio is the acceptance-corrected value, and 30% is the systematic error from the beam calculation. The errors in the backgrounds are the errors in calculating the backgrounds combined with the statistical error in the background.

At this stage of the analysis, we want to study the systematic errors in the beam calculation, our event selection, and event reconstruction before we make any conclusions.

We would like to thank the members of the AGS staff for much valuable support, and in particular Dr. A. Carroll, for his perseverance with the horn system. This work was supported by NSF Grants PHY86-10898, and PHY86-19556, and by the U. S. Department of Energy, under contract DE-AC02-76ERO1195.

References

- 1) "Major Detectors in Elementary Particle Physics", LBL-91 supplement.
- 2) W. R. Nelson, H. Hirayama, and W. O. Rogers, "The EGS4 Code System", SLAC-Report-265 (1985).
- 3) N. Kondakis, contribution to these proceedings.